Çukurova Üniversitesi Mühendislik Mimarlık Fakültesi Dergisi, 35(2), ss. 369-378, Haziran 2020
Çukurova University Journal of the Faculty of Engineering and Architecture, 35(2), pp. 369-378, June 2020

Experimental Investigation of the Flow Characteristics around a NACA0012 Airfoil Subjected to Stall and Post-Stall Conditions

Göktürk Memduh ÖZKAN[*1]

[1]*Çukurova University, Faculty of Engineering, Department of Mechanical Engineering, Adana*

Geliş tarihi: 08.05.2020 Kabul tarihi: 30.07.2020

Abstract

The flow structure and turbulent characteristics of an airfoil at various Reynolds numbers (Re_c = 1.5×10^4, 2.0×10^4, 2.5×10^4) have been investigated considering two angles of attack (α = 10^o and α = 12^o). PIV measurements have been performed and time-averaged and instantaneous results were presented utilizing vorticity, profiles of streamwise velocity, Reynolds shear stress, and turbulent kinetic energy distributions. The results have shown that both the Re_c and α significantly affect the flow characteristics around the airfoil. Furthermore, the change in flow characteristics between the stall and post-stall angles was elaborated and compared with each other, as being in good agreement with the available literature. The turbulent fluctuations in the airfoil wake, as well as in the suction side, were obtained to be more intense at post-stall angle compared with the stall condition. Besides, due to the earlier flow separation, post-stall condition presented a larger wake and the shedding of vortices formed by the leading and trailing edges of the airfoil.

Keywords: Airfoil, Stall, PIV, Flow structure

Stol ve Stol Ötesi Durumlara Maruz Kalan Bir NACA0012 Kanat Profili Etrafındaki Akış Karakteristiklerinin Deneysel İncelenmesi

Öz

Bir kanat profilinin akış yapısı ve türbülans özellikleri, çeşitli Reynolds sayılarındaki (Re_c =$1{,}5\times10^4$, $2{,}0\times10^4$, $2{,}5\times10^4$) iki atak açısı (α=10^o ve α=12^o) göz önüne alınarak incelenmiştir. PIV ölçümleri gerçekleştirilmiş ve zaman ortalamalı ve anlık girdap, akış hızı profilleri, Reynolds kayma gerilmesi ve türbülans kinetik enerji dağılımları kullanılarak sonuçlar sunulmuştur. Sonuçlar, hem Reynolds sayısının hem de hücum açısının, kanat profili etrafındaki özelliklerini önemli ölçüde etkilediğini göstermiştir. Stol ve stol ötesi açılarda akış karakteristiklerindeki değişiklik, mevcut literatürle iyi bir uyum içinde detaylandırılmış ve birbirleriyle karşılaştırılmıştır. Hem kanat profili art izinde hem de emme yüzeyinde oluşan türbülans çalkantılarının, stol ötesi açıda daha şiddetli olduğu elde edilmiştir. Bunun yanında, daha erken akış ayrılması sebebiyle stol ötesi durum, kanat profilinin hücum ve firar kenarlarından doğan girdapların kopması ile birlikte daha geniş bir art izi yapısı göstermiştir.

Anahtar Kelimeler: Kanat profili, Stol, PIV, Akış yapısı

[*]Corresponding author (Sorumlu yazar): Göktürk Memduh ÖZKAN, *gmozkan@cu.edu.tr*

1. INTRODUCTION

The stall condition of an airfoil is a subject of interest due to its importance in aerodynamics, and turbomachinery applications (propellers, turbines). When the flow separates from the leading edge at sufficiently large angle of attack, α, oscillations in the velocity and pressure (on the suction side) may occur, resulting in high amplitude vibrations on the airfoil. The consequences of stall may be an airplane crash or reduced efficiency of a turbomachine. The responsible mechanism for stall behavior has been reported by various researchers [1-3], i.e., at large attack angles, α, laminar separation bubble (LSB) formed on the airfoil's suction side starts bursting and cannot reattach to the airfoil's upper surface. However, the dynamics of the flow based on the separation mechanism under stall remain not fully understood and need further investigations to improve engineering designs. Mainly three different stall types have been reported by McCullough and Gault [4]; trailing edge stall, leading-edge stall, and combined trailing-leading edge stall. Through them, the combined stall has the most detrimental effect on the aero-hydro dynamic characteristics of the engineering devices. The combined (or full) stall is realized when angle of attack approaches far beyond the post-stall angle of the airfoil.

On the other side, the low Reynolds number aerodynamics [5] have taken little attention on the research community and still need to be analyzed in detail due to its significance, especially on improving unmanned aerial vehicles [6], as well as the turbomachines. Wang et al. [7] have reported three flow regimes to present individual flow structures on the suction side of a NACA0012 airfoil. Ultra-low ($<10^4$), low (10^4-3.0×10^5), moderate (3.0×10^5-5.0×10^6) and high ($>5.0\times10^6$) Reynolds number flows were revealed in their research where eight distinct flow structures dependent on α, were described. Direct numerical simulations of Rodriguez et al. [3] observed that the structures of separated flow at two different stall angles are slightly different, and corresponding coherent structures also present different modes, in agreement with Huang and Lin [8]. It should be noted that these differences in flow structures still need to be further investigated in detail, and available numerical works should be supported by experimental studies. In this regard, stall and post-stall conditions of a NACA0012 airfoil at low Reynolds numbers are investigated by Particle Image Velocimetry with this study. Two angles of attack, $\alpha = 10^o$ and $\alpha = 12^o$ were considered at chord-based Reynolds numbers of $Re_c = 1.5\times10^4$, 2×10^4, 2.5×10^4. Through them, the results obtained at $Re_c = 2.0\times10^4$ were further elaborated since, at this Reynolds number, $\alpha = 10^o$ and $\alpha = 12^o$ correspond to stall and post-stall angles, respectively for the NACA0012 airfoil according to [7, 9, 10]. It is hoped from this study that the presented results may be beneficial to contribute to the knowledge on low-Reynolds number aero-hydrodynamics prone to stall conditions regarding various engineering applications.

2. EXPERIMENTAL METHOD

The experiments were performed in a closed-loop water channel which has an 8 m-long test section with a spanwise dimension of 1 m and a height of 0.75 m. The turbulence intensity of the free stream velocity at the measurement plane is measured to be less than 2%. For the airfoil, one of the most studied shapes in the literature, NACA0012, was selected and manufactured utilizing 3D printing. High surface quality was obtained by a final polishing of the surface. The airfoil has a chord length of c=0.1 m and a span of b=0.2 m which corresponds to an aspect ratio of $AR=b/c$=2. Endplates with this AR satisfy the spanwise uniformity of the flow, according to Boutilier and Yarusevych [11]. Hence, the airfoil was fixed with endplates, to eliminate the wall and wing-tip effects on the flow structure. The measurements were performed 5.5 m away from the inlet of the test section, and water height was kept constant as h_w=0.5 m. A table was used as the bottom endplate to locate the airfoil at the center of the test section to eliminate the effect of the turbulent boundary layer developed on the side and bottom walls (see Figure 1). The coordinate system was located as started by the leading edge of the airfoil.

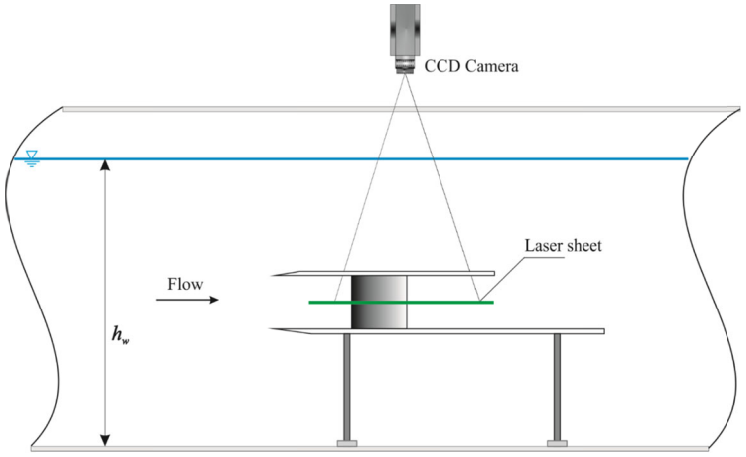

Figure 1. Schematic presentation of the experimental set-up from the side view

Two angles of attack were considered as α = 10° and α = 12° at three different Reynolds numbers based on the chord length, Re_c = 1.5×10^4, 2.0×10^4, 2.5×10^4 ($Re_c = U_\infty c/\nu$ where U_∞, c, and ν are the free-stream velocity, chord length, and kinematic viscosity, respectively). The angle of attack was adjusted using a Vernier protractor printed on the upper endplate and checked with the camera in the PIV system to ensure that the angle was correctly adjusted. The uncertainty in the angle of attack was ε_α=±0.1°. The temperature of the water was measured and kept constant as T=22.8 °C, corresponding to a kinematic viscosity of ν=0.9427×10^{-6} m^2/s [12]. Particle Image Velocimetry (PIV) technique was used to measure the two-dimensional velocity field on the suction side of the airfoil and its near wake. A 35 mm Nikon lens at f /4.0 was mounted on the Flow Sense 2ME camera (CCD, 2M, 1600×1200 pix resolution, 8-bit dynamic range, 7.4 µm pixel size) to capture the particle images. Silver coated particles having 10 µm diameter were used for seeding the flow. A double-pulsed Nd: YAG laser having 532 nm wavelength and 120 mJ/pulse output with a repetition rate of 15 Hz was used for the illumination. The laser sheet thickness and time between images were adjusted to 1 mm and 1000 µs, respectively. One thousand images were captured for each measurement, and the Dynamic Studio software package was utilized for cross-correlation analysis. For rejecting or substituting spurious vectors (less than 2%), the universal outlier detection technique [13] was utilized by applying a normalized median validation using a single detection threshold. The uncertainty in measurements [14] was about 2% relative to free-stream velocity in the measurement plane. The vorticity magnitudes were computed by flow circulation using the method of Landreth and Adrian [15]. An interrogation window size of 32×32 pixels was employed with a 50% overlap. The magnification of M=0.065, yielding a resolution of 8.75 px/mm in the object plane, was considered for all experiments, corresponding to the final field of view with 183×137 mm^2.

3. RESULTS AND DISCUSSION

The structure of the flow around airfoils strongly depends on Re_c and α, resulting in variations on separation, reattachment, and transition mechanisms that determine the wake characteristics of the airfoil. Therefore the effect of Re_c on the flow structure of airfoil at angles of attack of α=10° and α=12° is presented in Figure 2 and 3, respectively to elaborate the airfoil wake utilizing time-averaged, $<\omega>$and instantaneous, ω spanwise vorticity contours which were normalized by the chord length, c and the free-stream velocity, U_∞. It can be seen from Figure 2 that the shear layer separates from the leading edge at Re_c=1.5×10^4, resulting in Kelvin-Helmholtz instability followed by roll-up of the

vortices along the suction side which may be considered as partially attached boundary layer according to Wang et al. [7]. This behavior can also be seen by the time-averaged vorticity contours, $<\omega>$, where a distinct structure of the upper shear layer is observed along the leading edge. Due to the increased momentum of the flow by increasing Re_c, the separation is shifted with slight oscillations on the airfoil surface for $Re_c > 1.5\times10^4$. While evident perturbations exist in vortical structures at $Re_c=2.0\times10^4$, the flow is more likely to keep attached at $Re_c=2.5\times10^4$. This behavior is due to the particular condition of $\alpha = 10^o$ at $Re_c = 2.0\times10^4$, which was defined as the stall angle by previous studies [7,9] for NACA0012. The flow is almost stable and attached at $Re_c=2.5\times10^4$ since the flow separation is postponed due to the increased momentum of the free stream flow. It should also be noted that lower shear evolving from the trailing edge is not strong enough to entrain into the airfoil wake and loses intensity by increasing Re_c. Therefore, even slight oscillations occur in the airfoil wake; vortex shedding could not be observed at the current field of view.

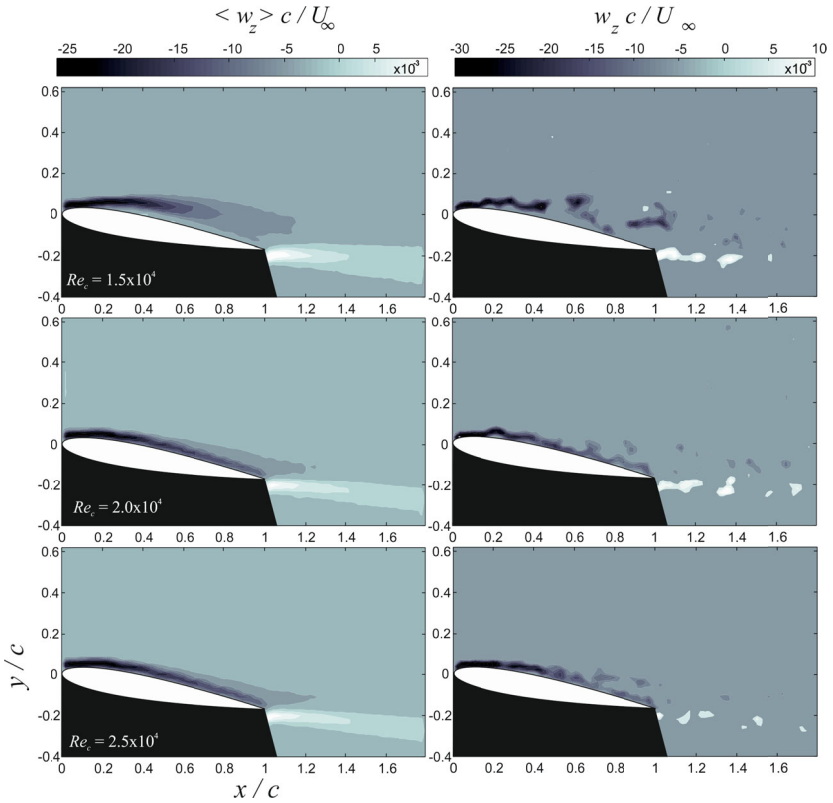

Figure 2. The variation of time-averaged (left) and instantaneous (right) spanwise vorticity contours at $\alpha=10^o$ for the specified Re_c range

Based on the results presented in Figure 2, the flow structures obtained at $\alpha = 10^o$ indirectly validate the present experiments. Hence the case at $Re_c = 2.0\times10^4$ can be considered as a stall point and will be elaborated in detail latter through the manuscript. To compare the flow structures and turbulent characteristics at $\alpha = 10^o$, the angle of attack of $\alpha = 12^o$ can also be considered as the post-stall angle of attack. In this regard, the time-averaged and instantaneous vorticity contours are presented in Figure 3 at $\alpha=12^o$ by varying Re_c. It is evident from the figure that almost all cases, the

flow separation takes place at the leading edge. At Re_c=1.5×10^4, a reattachment cannot be seen, and interaction of the vortices generated by the leading and trailing edges exists in the near wake of the airfoil. This is in good agreement with the case of α=10^o under the same Re_c where the momentum of the flow is not adequate for the reattachment. An increase in Re_c to Re_c=2.0×10^4 results in a delayed separation on the upper surface, which can be understood from both time-averaged and instantaneous vorticity distributions. Compared with the case of α=10^o, complete separation is obtained as expected from the flow physics, i.e., at post-stall angles, full separation of the flow should take place on the suction side of the airfoil. However, it can be seen from the instantaneous vortices that the flow intermittently reattaches on the airfoil, which is an indication of strong unsteady oscillations under post-stall conditions. Further increase in Reynolds number to Re_c=2.5×10^4 shows a more clear generation of the upper shear layer along the leading edge, which slightly enrolls into the suction side due to the increased momentum of the flow. It should be noted that the roll-up of the lower shear layer from the trailing edge does not take place for Re_c=2.0×10^4 and Re_c=2.5×10^4, which was the case for Re_c=1.5×10^4. This might be due to the rapid breakdown of the vortices when the momentum is more considerable at higher Re_c.

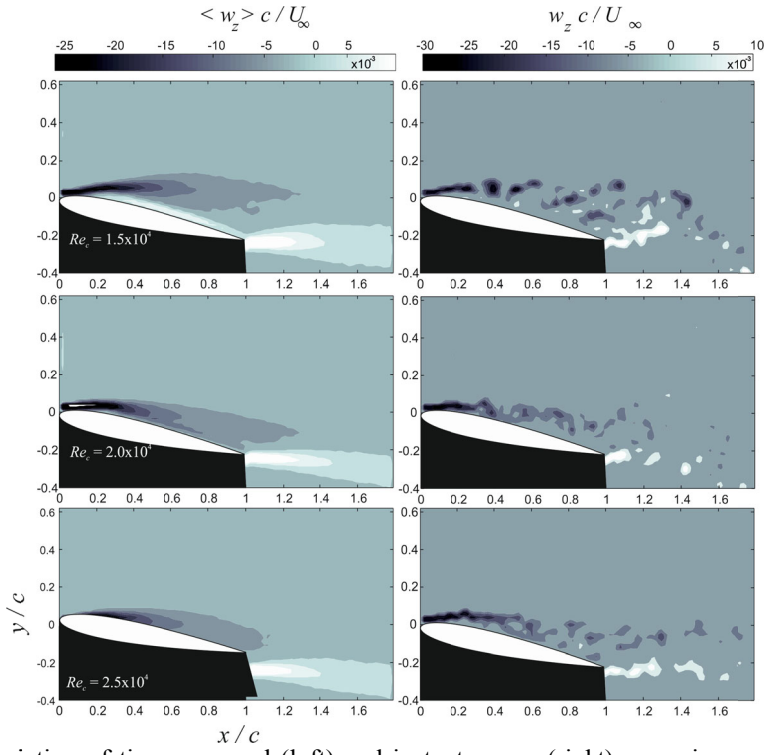

Figure 3. The variation of time-averaged (left) and instantaneous (right) spanwise vorticity contours at α=12^o for the specified Re_c range

The change in streamwise velocity distribution in the transverse flow direction is presented in Figure 4, where the velocity magnitudes were normalized by the free-stream velocity, U_∞. The angles of attack of α = 10^o and α = 12^o were presented on the top and bottom of Figure 4, respectively for all Re_c numbers at streamwise locations of x/c = 0.5 and x/c = 1.0. At both locations, Re_c =1.5×10^4 shows a larger momentum deficit compared with greater Re_c numbers according to the stronger flow separation. This condition is seen at x/c = 1.0, which is the edge of

the trailing edge. Profiles of Re_c x/c = 2.0×10^4 and Re_c =2.5×10^4 are almost identical at both streamwise locations presenting that the flow is more likely to be attached to the airfoil due to the increased momentum.

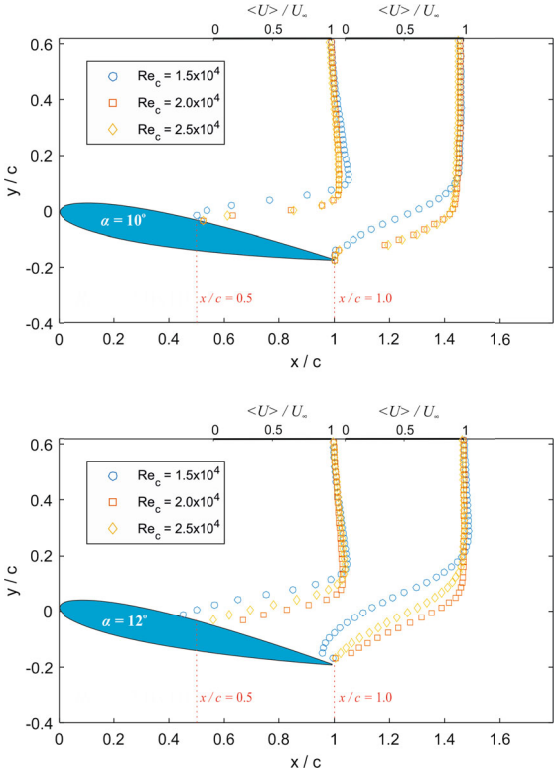

Figure 4. Time-averaged streamwise velocity profiles, $<U>/U_\infty$ normalized with free-stream velocity at streamwise locations of x/c=0.5 and 1.0 for all Re_c

The angle of attack of α=12° is presented at the bottom of Figure 4. Since the flow separation is earlier and reattachment is not possible at this angle, the negative magnitudes of the streamwise velocity are more distinguishable at Re_c=1.5×10^4. Unlikely with α = 10°, here there is a distinct difference in the profiles of Re_c=2.0×10^4 and Re_c=2.5×10^4 even they both present positive magnitudes at specified locations. Interestingly, the momentum of Re_c=2.0×10^4 is greater compared with Re_c=2.5×10^4, which are considered as post-stall conditions. This might be due to the faster breakdown of vortices separated from the leading edge at Re_c=2.5×10^4, whereas the separated vortical structures found more likely to be attached on the airfoil surface at Re_c=2.0×10^4. According to these results presented in Figure 4, the largest deficit in the momentum is obtained at the lowest Re_c. However, the least momentum deficit is obtained at Re_c=2.0×10^4, as the post-stall angle for this airfoil type [9]. Therefore, it can be concluded that at post-stall angles, there is no direct relationship between the momentum deficit and Re_c, the lower deficit is obtained exactly at the post-stall angle.

The conclusion by Figure 4 can further be verified by the wake velocity profiles. In this regard, the distribution of wake velocity profiles for all Re_c at α=10° and α = 12° are presented in Figure 5 at x/c=1.5. Here, the profiles on the suction side are in accordance with the wake velocity profiles in which the cases for Re_c>1.5×10^4 exhibit identical shape with lower momentum deficit compared with Re_c=1.5×10^4. Furthermore, α=12° presents the largest deficit at Re_c=1.5×10^4, where the flow separation is almost at the leading edge. Meanwhile, the smallest momentum deficit is observed for Re_c=2.0×10^4, as can be considered as a special characteristic of post-stall angles. Henceforward, turbulent characteristics of the flow only at the stall and post-stall angles will be considered to elaborate on their special conditions. From now on, the term stall and post-stall conditions will be used for the conditions α=10° and α=12°, respectively, at Re_c=2.0×10^4.

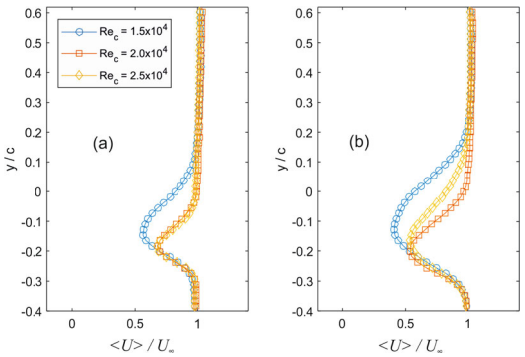

Figure 5. Time-averaged streamwise velocity profiles, $<U>/U_\infty$ at streamwise locations of x/c=1.5 at (a) α=10° (b) α=12°

Turbulent kinetic energy, $<k>$, can be approximated by two-dimensional flow assumption by Sheng et al. [16] and is utilized to consider the fluctuations in all directions. The following formula was used to calculate the turbulent kinetic energy where the third fluctuating component is considered to be equal to the half of $(<u'u'>+<v'v'>)$ (Equation 1).

$$<k>=\frac{3}{4}(<u'u'>+<v'v'>) \quad (1)$$

The spatial distributions of turbulent kinetic energy, $<k>$ together with Reynolds shear stress, $<u'v'>$ are presented in Figure 6 for stall and post-stall conditions. Their magnitudes were normalized with the square of free-stream velocity, U_∞^2, where the minimum and incremental values of $<k>$ were taken as 0.02 and 0.01, respectively. For $<u'v'>$, a color bar is included as an inset to the figure. The contour distributions of $<k>$ at stall show the highest concentration along the airfoil's upper surface, which is due to the separation from the leading edge followed by reattachment and consequent oscillations along the surface. The high fluctuations on the suction side consequently result in kinetic energy production in the airfoil wake. This situation can be seen by the distribution of $<u'v'>$ where a negative cluster and a positive cluster are formed along the leading and trailing edges, respectively. Such kind of positive-negative $<u'v'>$ distribution is indicative of possible interaction of the vortices and consequent vortex shedding downstream of the airfoil. The structure is changed when the α increased to the post-stall condition shown at the bottom of Figure 6. It should be noted that at post-stall angle, the area occupied by both $<k>$ and $<u'v'>$ increases, indicating that the wake region gets larger compared with the stall angle. This is also clear with the concentrations on the suction side in which they are weaker for the post-stall condition. Furthermore, the magnitude of the maximum positive shear stress, $<u'v'>$ increased by 66.7% compared with the post-stall case (the exact magnitudes are shown in the figure). This sudden increase very well explains the transition of turbulent flow characteristics from stall to post-stall conditions.

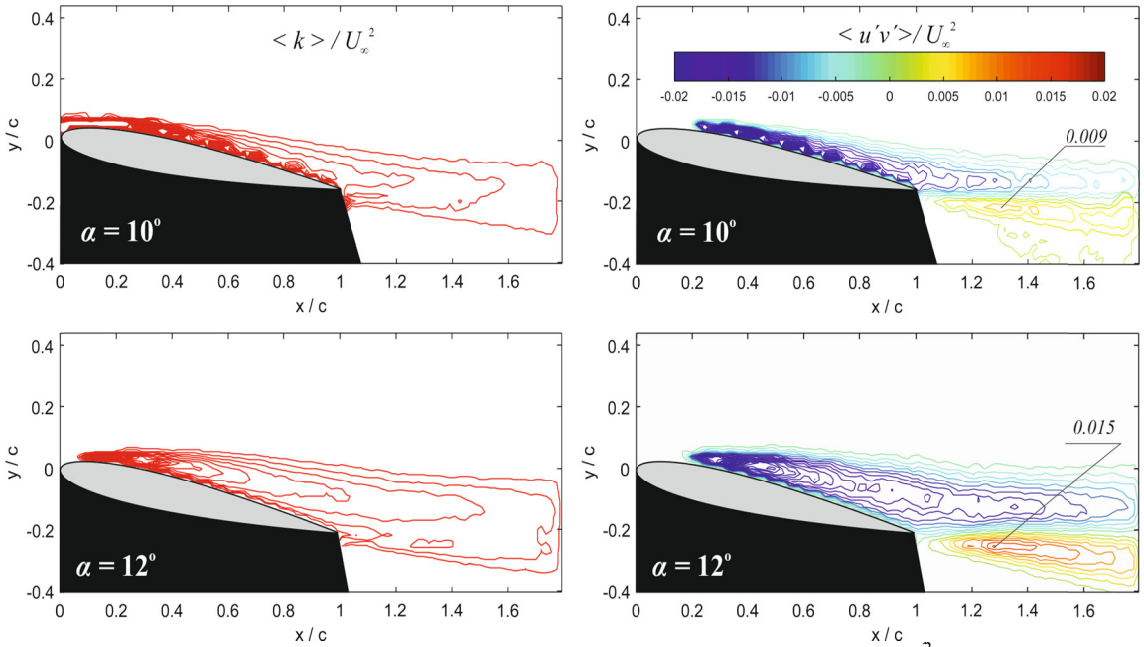

Figure 6. Spatial distribution of the time-averaged turbulent kinetic energy, $<k>/U_\infty^2$ and Reynold shear stress, $<u`v`>/U_\infty^2$ for stall and post-stall angles

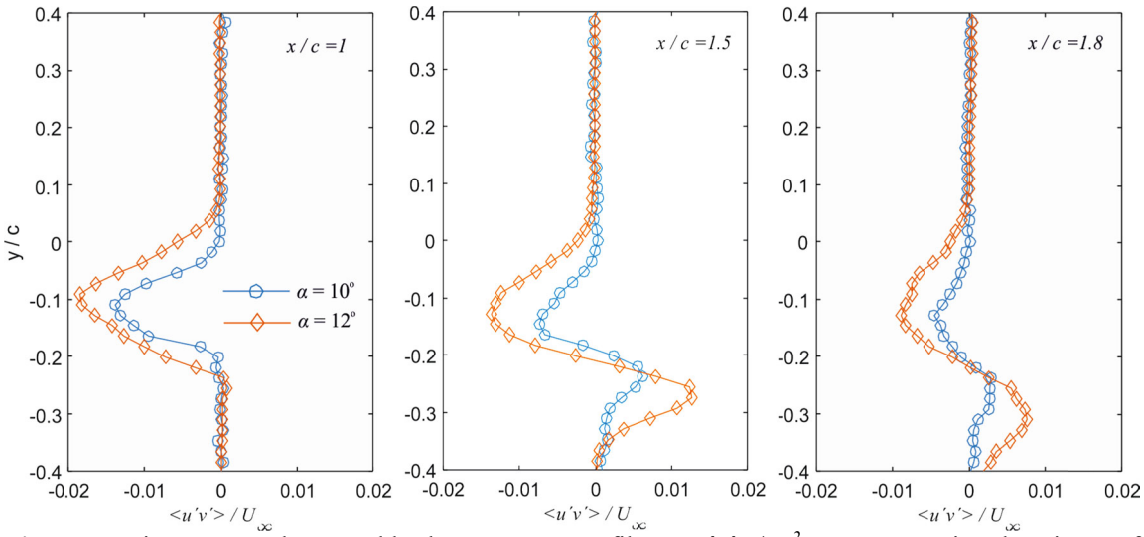

Figure 7. Time-averaged Reynold shear stress profiles $<u`v`>/U_\infty^2$ at streamwise locations of x/c = 1.0, 1.5 and 1.8 at stall and post-stall angles

To present the changes in the wake of airfoil more quantitatively, the profiles of normalized $<u`v`>$ magnitudes are presented in Figure 7 at three streamwise locations in the airfoil wake, for both angles. One can see that the magnitudes are higher for post-stall conditions at all locations, as expected, i.e., a greater separation causes a larger momentum deficit as depicted before, hence more substantial momentum transfer between the shear layers. The positive and negative $<u`v`>$ magnitudes are almost symmetrical for all locations, finally approaching zero magnitudes in the free-stream flow. It should also be noted that the values tend to decrease by increasing streamwise direction where the highest value is observed for x/c=1.0 (considering the airfoil wake). The physics behind this reduction can be explained by the dissipation of turbulent kinetic energy in the streamwise direction, which was created by the interaction of vortices generated by the leading and trailing edge shear layers. This is further elaborated in Figure 8, which depicts the trend in $<k>$ downstream of the airfoil at a transverse location of y/c=0.0. For x/c> 1.0, it is observed that $<k>$ is higher at post-stall condition; however, the magnitudes of both conditions tend toward to almost zero and get the same value at x/c=1.4. Furthermore, Figure 8 also reveals information for the suction side, i.e., the magnitude of $<k>$ is greater for stall condition and decreasing in the downstream direction. The magnitudes for stall and post-stall get the same magnitude at about x/c=0.6, and the condition is now reversed, i.e., the magnitude of $<k>$ for post-stall is greater. Similar to the comments on $<u`v`>$ profiles shown in Figure 7, this is due to the strong separation from both leading and trailing edges followed by the vortex roll-up and consequent vortical interactions downstream of the airfoil wake. The presented results are in good agreement with the vorticity contours presented in Figures 2 and 3, as well as the results of Huang and Lin [8].

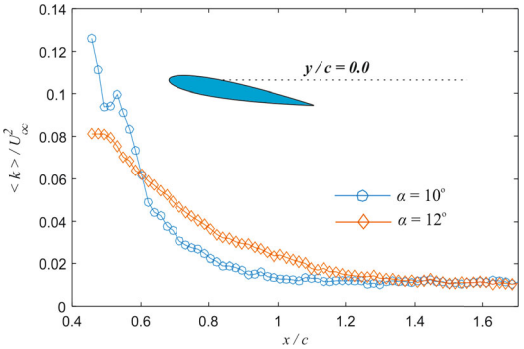

Figure 8. Change in normalized turbulent kinetic energy, $<k>/U_\infty^2$ in streamwise direction at transverse location of y/c=0.0

4. CONCLUSIONS

In this study, PIV measurements were performed around a NACA0012 airfoil to examine the effect of Reynolds number on the flow characteristics, as well as the change in turbulent fluctuations at stall and post-stall angles. A total of six cases were considered for the study having α=10^o and α=12^o angle of attack and Reynolds numbers of Re_c=1.5×10^4, 2×10^4, 2.5×10^4. According to the results obtained, it is found that the effect of Re_c on the flow structure is predominantly observed for α=12^o, i.e., the separated flow region was larger, and the turbulent fluctuations were more significant compared with α=10^o. At post-stall angles, it was revealed that there is no direct relationship between the momentum deficit and Re_c according to the velocity profiles evaluated on the suction side, as well as the airfoil wake.

Throughout the parameters, the considered angles corresponded to stall and post-stall conditions of the airfoil at Re_c=2.0×10^4 and results were found to be in consistent with Celaver et al. [9] and Wang et al. [7]. The transition from stall to post-stall was unveiled quantitatively. It was shown that the turbulent fluctuations dramatically change from stall to post-stall angle in which a significant increase in their magnitudes occurs for the post-stall condition. An increase of 66.7% in the maximum Reynolds shear stress was obtained at post-stall angle compared with the stall angle which is due to the earlier and massive separation of the flow. The underlying mechanism of greater turbulent fluctuations at post-stall angle was explained by the formation of the vortices evaluated at the leading and trailing edges, finally interacting with each other. Eventually, vortex shedding was observed at post-stall angles, which can induce the vibrations on the airfoil.

It is hoped that the results of the present work might help to understand the physical mechanism of stall conditions in airfoils. Besides, this study may be extended further to investigate the vortex shedding characteristics, especially at post-stall angles.

5. REFERENCES

1. Almutairi, J., Jones, L., Sandham, N., 2010. Intermittent Bursting of a Laminar Separation Bubble on an Airfoil. AIAA Journal 48 (2), 414–426.

2. Bragg, M., Heinrich, D., Balow, F., Zaman, K., 1996. Flow Oscillation Over an Airfoil Near Stall. AIAA Journal 34 (1), 199–201.

3. Rodriguez, I., Lehmkuhl, O., Borrell, R., Oliva, A., 2013. Direct Numerical Simulation of a NACA0012 in Full Stall. International Journal of Heat and Fluid Flow. 43, 194- 203.

4. McCullough, G.B., Gault, D.E., 1951. Examples of Three Representative Types of Airfoil Section Stall at Low Speeds. NACA TN No: 2502.

5. Lissaman, P.B.S., 1983. Low-Reynolds Number Airfoils. Annual Review of Fluid Mechanics, 15, 223-39.

6. Mueller, T.J., DeLaurier, J.D., 2003. Aerodynamics of Small Vehicles. Annu. Rev. Fluid. Mech. 35(1), 89–111.

7. Wang, S., Zhou, Y., Alam, M.M. Yang, H., 2014. Turbulent Intensity and Reynolds Number Effects on an Airfoil at Low Reynolds Numbers, Physics of Fluids, 26, 115107.

8. Huang, R.F., Lin, C.H., 1995. Vortex Shedding and Shear-layer Instability of Wing at Low-Reynolds Numbers. AIAA Journal 33 (8), 1398-1403.

9. Cleaver, D.J., Wang, Z., Gursul, I., Visbal, M., R., 2011. Lift Enhancement by Means of Small-amplitude Airfoil Oscillations at Low Reynolds Numbers. AIAA J. 49(9), 2018–2033.

10. Yasuda, T., Fukui, K., Matsuo, K., Minagawa, H., Kurimoto, R., 2019. Effect of the Reynolds Number on the Performance of a NACA0012 Wing with Leading Edge Protuberance at Low Reynolds Numbers. Flow, Turbulence and Combustion. 102, 435-455.

11. Boutilier, M.S.H., Yarusevych, S., 2012. Effects of end Plates and Blockage on Low-Reynolds-number Flows Over Airfoils. AIAA J. 50, 1547.

12. Cengel, Y.A., Cimbala, J.M., 2008. Fluid Mechanics: Fundamentals and Applications (1st Edition), McGraw Hill, 49.
13. Westerweel, J., Scarano, F., 2005. Universal Outlier Detection for PIV Data. Experiments in Fluids, 39, 1096–1100.
14. Raffel, M., Willert, C.E., Scarano, F., Kähler, C.J., Wereley, S.T., Kompenhans, J., 2018. PIV Uncertainty and Measurement Accuracy. In: Particle Image Velocimetry. Springer, Cham.
15. Landreth, C.C., Adrian, R.J., 1990a. Impingement of a Low Reynolds Number Turbulent Circular Jet onto a Flat Plate at Normal Incidence. Experiments in Fluids, 9, 74-84.
16. Sheng, J., Meng, H., Fox, R.O., 2000. A large eddy PIV method for turbulence dissipation rate estimation. Chem. Eng. Sci., 55, 4423-4434.